Measurement 221 (2023) 113460

Contents lists available at ScienceDirect

Measurement

journal homepage: www.elsevier.com/locate/measurement

Twisting torque – A simplified theoretical model for bicycle tyres

G. Dell'Orto *, F.M. Ballo, M. Gobbi, G. Mastinu

Department of Mechanical Engineering, Politecnico di Milano, Via La Masa 1, 20156 Milan, Italy

ARTICLE INFO

Keywords:
Self-aligning torque
Lateral characteristics
Modeling
Mobility
Sustainability

ABSTRACT

In this paper, the twisting torque of bicycle tyres is studied. The twisting torque is just the self-aligning torque for null lateral slip and non-null camber. The relationship between twisting torque and contact patch area has been analyzed. As the latter increases, twisting torque increases as well. A theoretical model to evaluate twisting torque has been implemented. Since twisting torque is mainly due to longitudinal slip in cambered wheel, increasing the contact patch area the stresses are located at a larger distance from the median plane of the contact patch. The resulting torque will be higher in magnitude.

Finally, the model has been validated comparing the outcomes with the experimental data, with a mean error less than 3% for camber angles less than 10°.

1. Introduction

Climate-change requires governments to take action to reduce pollutant emissions. In this context, transportation sector is a relevant source of pollution. It is responsible of one-third of all energy in EU and accounts for more than one-quarter of total EU greenhouse gas emissions [1]. We need alternative and low-impact ways of mobility, and cycling may be a simple and cost-effective solution [2 3]. In addition, the current increasing cost of carbon fossil fuels [4] is forcing to reduce their use, so speeding up the process of conversion throw a more sustainable mobility.

An increase in the use of bicycles is expected in the close future [5 6], so that concerns about road safety are growing as well [7 8]. This aspect will force designers to find new feasible solutions for improving safety, performances [9] and comfort [10 11]. Advanced numerical models are required to study bicycle dynamics, nonetheless they usually ignore tyre dynamics and need to be complemented with realistic tyre models [12,13].

Tyres are important for bicycle handling [14]–[16]. Despite this, very few studies were focused on bicycle tyre characterization [12 17] and only few researchers have presented test-rigs for bicycle tyres [12]. In [18], they use a test-rig for motorcycle tyres adapted to accommodate bicycle tyres. Three different prototypes were also presented in [19]. Using one of them, it was possible to characterize mountain-bike tyres [15].

The dynamics of two-wheeled vehicles is featured by large camber angles, useful to generate lateral forces even with slip angle equal to zero [12 18]. The influence of camber angle on the mechanical characteristics must be properly addressed to fully characterize tyres. Nonetheless, no studies on twisting torque for bicycle tyres seem to have been carried out, being the research mainly focused on motorcycle tyres [20–23]. According to Pacejka [24], the self-aligning torque is different from zero when slip angle set to zero degrees, just for the camber effect. The relationship between the contact patch and twisting properties was stated in [25]. It was discovered the increase in magnitude of the twisting torque with the increase in contact patch area. This was also confirmed in [26]. They measured motorcycle tyre properties for different inflation pressures, also concluding the almost linear relationship between twisting torque and camber angle. An increase in inflation pressure led to decrease in twisting torque, since it changed the contact patch [27]. Self-aligning torque and twisting torque are the main responsible of yaw moment [28]. Furthermore, twisting torque has a relevant effect on steering torque, decreasing the effort required to driver leaning into a curve [29].

We would like to know if the same conclusions are valid also for bicycle tyres. The latter share with motorcycle tyres the toroidal shape of cross section [28], but they differ a lot in terms of compound, layers and manufacturing process. These aspects may affect considerably the tyre behavior, so that a deep study is necessary. Twisting torque tends to reduce the radius of curvature during the turning maneuver [30]. It is relevant to predict this behavior because it may affect the maneuverability [29] and the feeling of riders when approaching a curve. They perceive a sort of "autosteer" as they are leaning into a curve [15]. Twisting torque depends on vertical load and inflation pressure, which,

* Corresponding author.
E-mail address: gabriele.dellorto@polimi.it (G. Dell'Orto).

https://doi.org/10.1016/j.measurement.2023.113460
Received 23 January 2023; Received in revised form 5 June 2023; Accepted 15 August 2023
Available online 16 August 2023

together, may strongly affect the area of contact patch [25].

In this paper, a simplified theoretical model for predicting the twisting torque of bicycle tyres is presented. The self-aligning torque was measured through the test-rig *VeTyT* [12 31,32] developed at the Department of Mechanical Engineering of Politecnico di Milano. The twisting torque was experimentally evaluated for camber angles up to 25° (Section 2). Then, a simplified model to predict the twisting torque for different vertical loads and inflation pressure was implemented in Section 3. The effectiveness of the model was verified comparing the outcomes with the experimental results (Section 4).

2. Experimental tests – Contact patch and twisting torque

In this Section, the device to measure the lateral characteristics of the tyre is presented. Then, the evaluation of contact patch and twisting torque is discussed.

2.1. VeTyT test-rig

In this study, the measurement of the lateral characteristics of the tyre was performed through *VeTyT*, a test-rig specifically designed to measure the mechanical characteristics of bicycle tyres [31]. The measuring procedure is now certified in accordance with the standard defined by ISO 9001–2015.

VeTyT consists of a rigid frame made of Aluminum 6060 T6, reinforced with plates and steel rods to ensure lightness and adequate stiffness (Fig. 2.1). It holds the tyre on top of a flat track, moved by a 5 kW three-phase asynchronous electric motor. The frame is connected to the ground by means of Watt's linkage (Fig. 2.2) and universal joint. Two load cells can measure the lateral force exchanged along the contact patch tyre/rolling surface, while a third load cell is used to constrain the rotation of the steered wheel during the dynamic test. It measures the reaction force given by the tyre, from which the self-aligning torque can be derived.

The whole chassis can be tilted to set the camber angle in the range $\pm$ 25°, while the slip angle α can be adjusted by rotating the steering shaft. Longitudinal axis, defined by the centre of Watt's linkage and

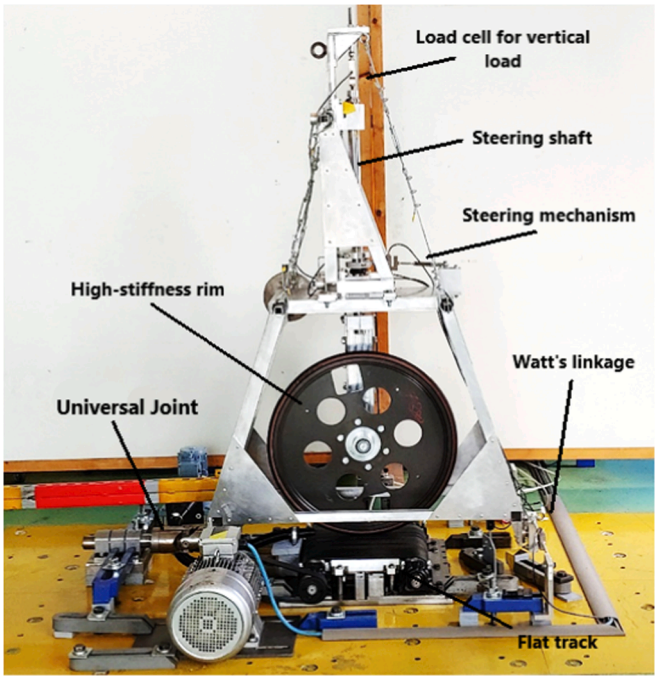

Fig. 2.1. . VeTyT test-rig at Politecnico di Milano. The frame carries the bicycle tyre on flat track. Here you can see the tyre mounted on high-stiffness laboratory rim.

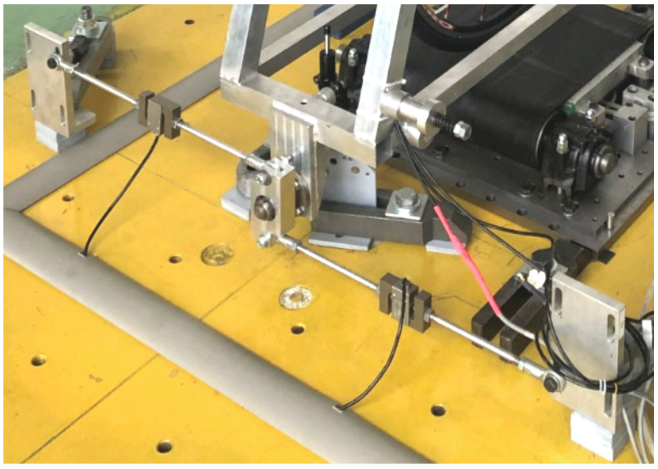

Fig. 2.2. . Watt's linkage used on VeTyT. The central part is connected to VeTyT, the rods with load cells are fixed to the ground. (adapted from [31]). It constrains the lateral motion, while it allows a limited vertical motion.

centre of universal joint, crosses the vertical axis (defined by steering shaft) in the contact tyre/rolling surface. In this way, we can set the camber angle while the contact patch always lying along the longitudinal axis. This allows both compensating the unevenness of rolling surface and ensuring zero longitudinal velocity of the contact point tyre/rolling surface. The vertical load acting on the wheel can be varied by adding masses on the frame. Its magnitude F_z is recorded by a load cell on the top of the steering shaft. The design solutions also allow changing the center of mass location due to added masses without affecting the measurements.

The complete assembly of the test-rig is shown in Fig. 2.1.

In this study, tests were performed on flat track covered with coarse sand (1.2 mm of granulometry). The speed was set to 6.1 m/s, found as optimal value to avoid the increase of temperature of the rolling surface.

The tyre was mounted on high-stiffness laboratory rim. In this way, the compliance of the rim does not affect the experimental measurements, being the lateral and radial stiffness of the rim much larger than the ones of the tyre. The lateral force was measured so as to derive the cornering stiffness. Twisting torque was derived from the measurement of self-aligning torque, setting the slip angle to 0° and varying the camber angle up to 25°.

2.2. Contact patch and twisting torque

Contact patch area may strongly affect the twisting torque [25,27], as stated in next Section 3. This is why it is necessary to evaluate the area and the shape of contact patch.

Contact patches were determined statically using sensitive pressure films. A 26 mm wide road bicycle tyre was tested for different inflation pressures and vertical loads. The dynamic measurement of contact patch is still really hard to implement to such a device designed for bicycle tyres. Systems based on image processing [33 34] or optical measuring system [35] have been recently presented but they still require large modifications on *VeTyT*.

Sensitive pressure films were scanned, and the area was calculated through the software ImageJ®. It is typically employed in the field of microbiology [3637], but it can be also used to measure contact patches, with a proper calibration of input images.

It is possible to note the increase in area as the vertical load increases, for the same inflation pressure. Similarly, contact patch area becomes larger with the increase of vertical load, keeping constant the inflation pressure.

Twisting torque was derived from the measurement of self-aligning torque through *VeTyT*. It corresponds to the self-aligning torque when

slip angle is equal to 0° and camber angle varies [30].

The tyre was mounted on high-stiffness rim and tested for different camber angles, inflation pressures and vertical loads. The results of an experimental campaign led with inflation pressure of 7.5 bar and vertical load equal to 490 N are depicted in Fig. 2.3 Each test was repeated three times, then averaged, resulting with a standard deviation of 2,5%. Because of the technical limitations to set exact null slip angle, the tests were repeated several times in then slip angle range $\pm$ 0.5°. Results were then linear interpolated in that range, to compensate for any detrimental errors which may occur when the forces to be measured are very small.

Self-aligning torque varies as function of slip and camber angle. In particular, when slip angle α is set to 0° the self-aligning torque is equal to the twisting torque. Practically, it means that the rider may feel a slight torque on the handlebar due to the camber effect. The twisting torque is depicted in Fig. 2.4 as function of camber angle γ.

Comparing the results with the ones for motorcycle tyres found in [24], the magnitude of the twisting torque is definitively smaller for bicycle tyres. We can note that twisting torque is one order of magnitude lower than the peak of self-aligning torque for the same camber angle. Remarkably, for motorcycle tyres it resulted of the same order of magnitude [38]. This may be due to the peculiar shape of contact patch for bicycle tyres, featured by large tyre diameter if compared to the width.

It was found a correlation between the twisting torque and the contact patch area. Larger contact patches imply higher difference in peripheral tyre speed, so locally different longitudinal slip values can be found within the contact patch. In Fig. 2.5 it is possible to observe the twisting torque measured for camber angle equal to 25°, for different contact patch areas (on x-axis). They were obtained varying inflation pressures (3.5, 5.5 and 7.5 bar) and vertical loads (400 N and 490 N). As the contact patch area increases also the twisting torque follows the same increasing trend. Experimental data have been fitted by a quadratic curve, as shown in Fig. 2.5 (dotted blue line).

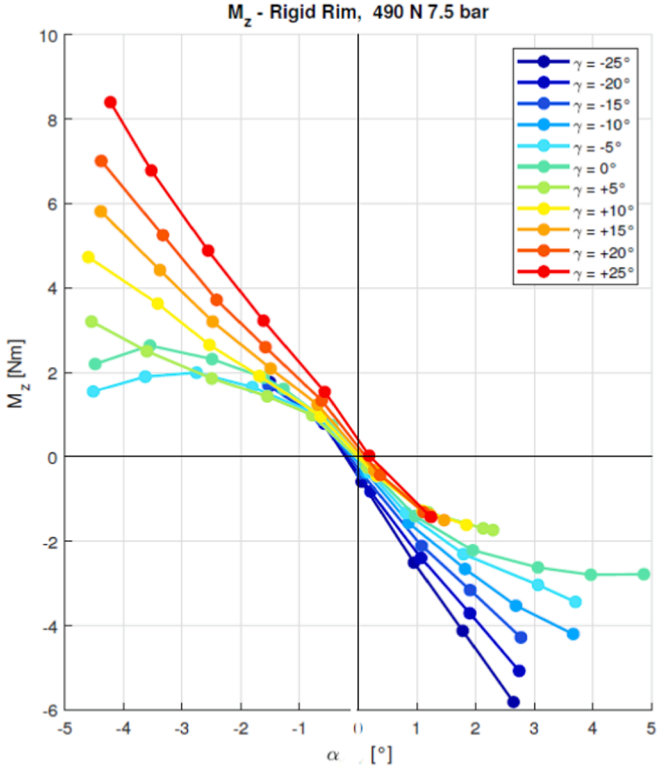

Fig. 2.3. . Self-aligning torque as function of slip angle. Results come from a test performed on 26 mm wide road racing tyre inflated at 7.5 bar and mounted on high-stiffness rim. A vertical load of 490 N was applied. Values were recorded for camber angles in the range −25° up to + 25°.

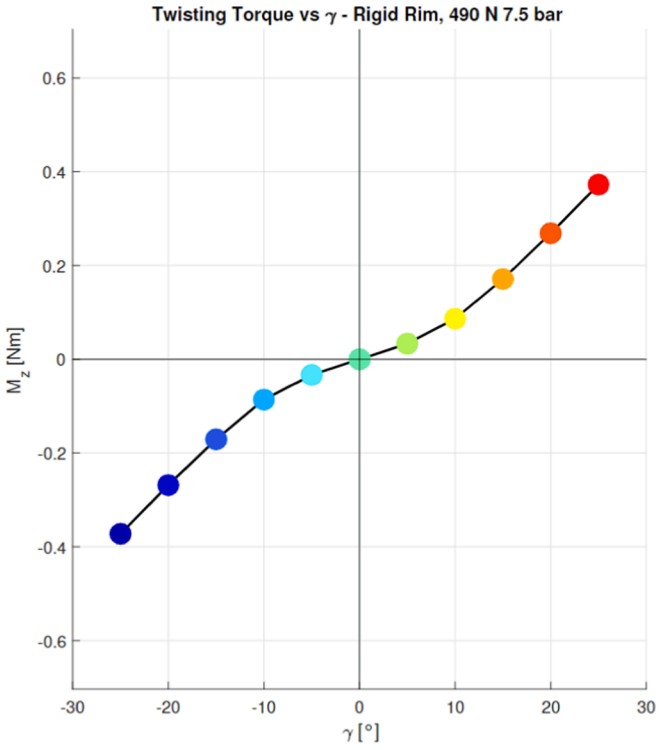

Fig. 2.4. . Twisting torque obtained from the test shown in Fig. 2.3. Values were recorded for camber angles in the range −25° up to + 25°. Colors are referred to the ones reported in Fig. 2.3.

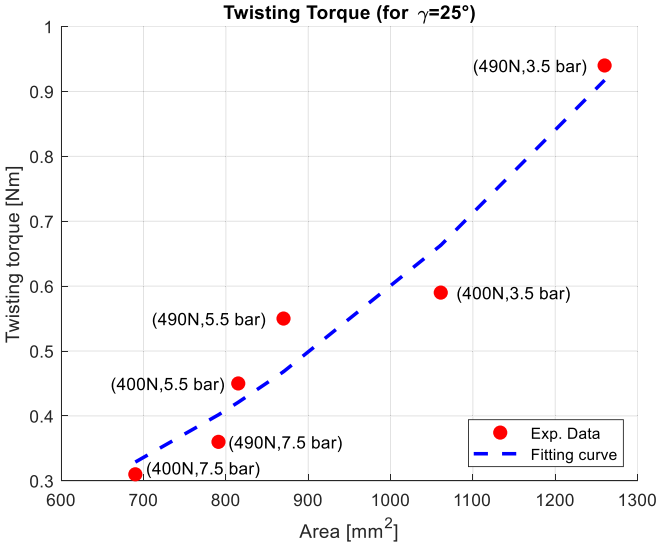

Fig. 2.5. . Twisting torque obtained for camber angle of 25° (y-axis), from tests on 26 mm wide road tyre. Different inflation pressures (3.5, 5.5 and 7.5 bar) and vertical loads (400 N and 490 N) were tested. It is depicted as function of contact patch area. Quadratic fitting curve is shown (blue dotted line, mathematical expression is: $y = 6.634(*10^{-7})x^2 - 0.0002613x + 0.1933$). (For interpretation of the references to colour in this figure legend, the reader is referred to the web version of this article.)

3. Model for twisting torque

In [30], the presence of longitudinal slip in the contact patch was found to be one of the causes of the twisting torque. The latter could be

strongly affected by the contact patch area since it varies with the pressure and vertical load [25 39].

The peripheral speed of a cambered free rolling tyre is not equal to the forward velocity at each location in the contact patch. Considering the wheel of Fig. 3.1 with an angular velocity ω, two different areas of stress level can be distinguished, featured by opposite stress levels and distance from the spin axis equal to r_A and r_B respectively ($r_A < r_B$). If r_0 is taken as the radius of the wheel along the median plane, we can consider a portion of the contact patch in which $r > r_0$ and a portion in which $r < r_0$ for the cambered wheel. Specifically, the longitudinal slip is positive where $r > r_0$, so that $\omega_r > \omega_{r_0}$. On the contrary, it is negative where $r < r_0$ (i.e.$\omega_r > \omega_{r_0}$). The longitudinal slip is responsible for the generation of longitudinal forces and a torque is generated around the centre of the contact patch.

In this paper, some assumptions have been made. The contact patch was considered elliptical even without varying in shape as camber angle increases. Then, longitudinal slip ε was assumed to vary linearly along transversal direction (*y* direction in Fig. 3.2). In this way, we can subdivide the contact patch into slices, and assume that a slice *dy* at a distance of *y* from the centerline of ellipse generates a force *dF* [24]. Similarly to the work presented by Pacejka in [24] for car tyres, we tried to evaluate the twisting torque as the integral of the infinitesimal force *dF* times the distance *y*, computed over the area (3.1). Reference system *x-y* was placed in the plane of the contact patch, where the *x-axis* defines the longitudinal direction and the *y-axis* the transversal one.

$$T = \int_A dF|y| \tag{3.1}$$

The radial distance between a generic point *P* belonging to the contact patch and the wheel spin axis can be expressed as follows (also refer to Fig. 3.3)

$$r(y) = r_0 + y\sin\gamma \tag{3.2}$$

Where γ is the wheel camber angle. The radial distance *r* is function of the coordinate *y* since we are considering the cambered wheel.

The longitudinal slip ε is positive for $y > 0$ and negative for $y < 0$ (Fig. 3.3), from which the longitudinal stress τ can be derived. It is defined according to (3.3).

$$\varepsilon = \frac{\omega r(y) - \omega r_0}{\omega r_0} = \frac{r(y) - r_0}{r_0} = \frac{r_0 + y\sin\gamma - r_0}{r_0} = \frac{y}{r_0}\sin\gamma \tag{3.3}$$

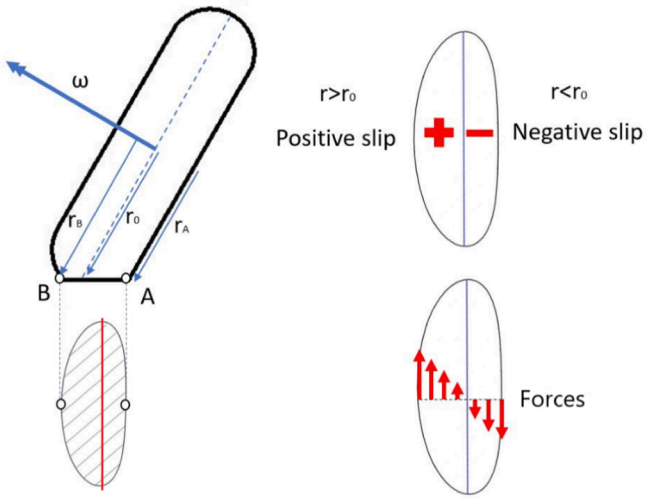

Fig. 3.1. . Cambered wheel with the distances between axis of rotation and the contact patch tyre/ground. The wheel is rotating at angular velocity ω. We can distinguish the points A and B on the lateral extremities of contact patch, featured by distances r_A and r_B from the spin axis of the wheel. r_0 is the radius of the wheel along the median plane.

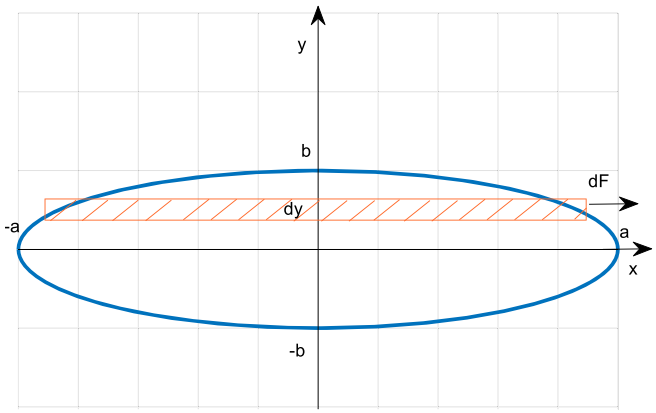

Fig. 3.2. . Top-view representation of the contact patch, with the reference system x-y with the origin in the centre of the ellipse. The slice of wide dy is at a distance y from the origin of axes.

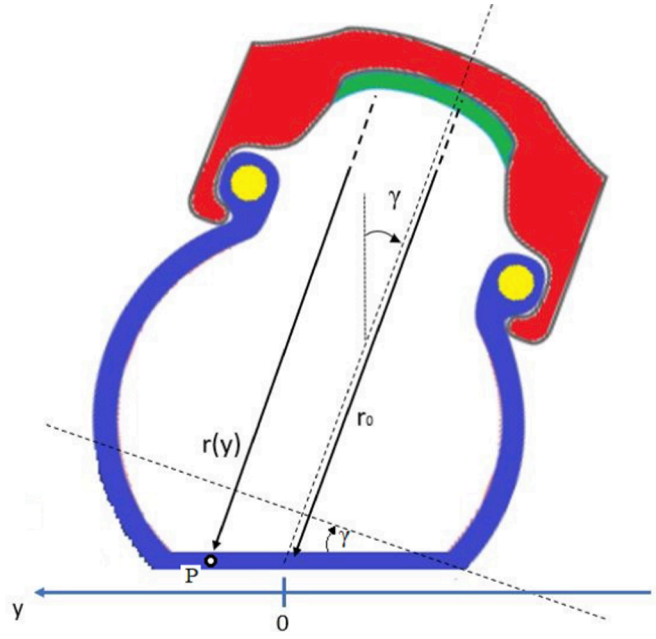

Fig. 3.3. . Schematic view of the cross section of cambered tyre. The angle γ is the wheel camber angle, while r(y) is the generic distance between a generic point P and the wheel spin axis. r_0 is the radius of the wheel along the median plane, which crosses the contact patch along the major axis of ellipse. The reference system x-y lays in the plane of the contact patch.

Since for limited values of slip (adhesion zone [40]) the longitudinal force F_x is linearly proportional to the longitudinal slip itself, we have

$$F_x = C_{F_x}\varepsilon \tag{3.4}$$

As first approximation, the longitudinal slip stiffness is assumed to be equal to the cornering stiffness [41].

$$C_{F_x} = C_{F_y} \tag{3.5}$$

The stresses τ can be expressed according to (3.6)

$$\tau = K_\varepsilon\varepsilon = K_\varepsilon\frac{y}{r_0}\sin\gamma \tag{3.6}$$

Where we have introduced the proportionality coefficient K_ε [N/mm^2]. It has been initially estimated as follows (terms *a* and *b* define the semi-major and semi-minor axis of the ellipse contact patch, see Fig. 3.2)

$$K_\varepsilon = \frac{C_{F_x}}{ab\pi} \tag{3.7}$$

The infinitesimal force dF is defined as the stress τ multiplied by the infinitesimal area $dA = 2xdy$, where dy is the width of the considered slice and $2x$ is the length (the slice is assumed to be a rectangle). In this way, we have

$$dF = \tau dA = \tau 2xdy \tag{3.8}$$

The term x can be written as function of y, since the contact patch was assumed to be elliptical by hypothesis.

$$x = a\sqrt{1 - \left(\frac{y}{b}\right)^2} \tag{3.9}$$

The infinitesimal force dF can be expressed as follows

$$dF = 2\tau a\sqrt{1 - \left(\frac{y}{b}\right)^2}dy \tag{3.10}$$

Because of the symmetry of the problem, the expression of twisting torque (3.1) can now be simplified in (3.11).

$$T = \int_{-b}^{b} dF|y| = 2\int_{0}^{b} dF|y| \tag{3.11}$$

Then, substituting with the expression found above, we have

$$T = 2\int_{0}^{b} 2\tau a|y|\sqrt{1 - \left(\frac{y}{b}\right)^2}dy \tag{3.12}$$

$$T = 2\int_{0}^{b} 2K_\varepsilon \frac{y}{r_0}\sin\gamma a|y|\sqrt{1 - \left(\frac{y}{b}\right)^2}dy \tag{3.13}$$

$$T = \frac{4a}{r_0}\sin\gamma \int_{0}^{b} y^2\sqrt{1 - \left(\frac{y}{b}\right)^2}dy \tag{3.14}$$

Solving the integral, the result is as follows

$$T = \frac{K_\varepsilon}{4r_0}\pi\sin\gamma ab^3 \tag{3.15}$$

The equation (3.15) has been derived referring to the contact patch. Analyzing the terms of (3.15), it can be stated that.

- The twisting torque T increases with the dimensions of the contact patch. The parameters a and b correspond to the semi-major and semi-minor axis of the ellipse which approximates the contact patch. Specifically, T increases linearly with respect to the length of contact patch (i.e. a), while it increases by a cubic factor with the width of contact (i.e. b).
- Twisting torque increases at increasing the camber angle γ (according to the term $\sin\gamma$).
- It is proportional to the longitudinal characteristics of the tyre through the term K_ε. A tyre with larger longitudinal slip stiffness will be featured by higher twisting torque.
- The twisting torque increases with the decrease in radius of the tyre r_0 [mm]. A tyre with reduced diameter will produce higher twisting torque with respect to a bigger one, if contact patch dimensions and longitudinal tyre properties are kept constant.

4. Model validation

Equation (3.15) was used to predict the twisting torque, then the results of the model can be compared with experimental data. The latter were derived from tests on test-rig *VeTyT*, for a 26 mm road racing tyre, mounted on high-stiffness rim with inner tube. It was tested for vertical load of 400 N and 490 N, for different inflation pressures (range from 3.5 to 7.5 bar). In this way, it is possible to have different contact patch areas and longitudinal stiffness. The contact patch areas were also measured for different conditions, as described in Section 2. The coefficient K_ε may vary with inflation pressure and vertical load, since tyre lateral characteristics and contact patch area change.

The model requires as input a single value of K_ε, so that it is necessary to develop a strategy to define a synthetic index, to simplify as much as possible the model. It was assumed a reference value of cornering stiffness $\overline{C_{F_y}} = 100N/^\circ$ coming from the mean value of many tests led on the same tyre with different vertical load and inflation pressure. Concerning the contact patch area, $\overline{A} = 906mm^2$ was considered as mean value of measurements under different conditions of vertical load and inflation pressure. The coefficient K_ε resulted as follows

$$K_\varepsilon = \frac{\overline{C_{F_y}}}{\overline{A}} = 6.3N/mm^2 \tag{4.1}$$

Looking at the results, it was noticed that the amplitude of twisting torque was always underestimated. To solve it, a least square method was used to define a factor to multiply the proportionality coefficient K_ε. A value of 6 was found to improve the matching between theoretical model and experimental data, as shown in Figs. 4.1 and 4.2 (obtained using a proportionality coefficient equal to $6K_\varepsilon$).

The theoretical model is able to provide curves sorted in very similar way. Referring to accuracy, the twisting torque estimated by the theoretical model corresponds to the measured one with a mean error less than 3% for low camber angles (<10°). The main difference is represented by the slope variation of the curves. The derivative of the measured twisting torque (Fig. 4.1) increases as the camber angle increases, while the derivative of estimated curves decreases with the increase in camber angle. This effect can affect the results for camber angles in the range 10-20°, since measured values present an increasing quadratic trend.

The difference in results may be explained by the approximations introduced in the model, such as the assumptions made on the shape of contact patch, the linear relationship between stress and slip and the possible slippage which may occur increasing the camber angle.

5. Conclusions

Twisting torque is relevant also for bicycle tyres, but significantly reduced in magnitude with respect to motorcycle tyres. Nonetheless, it may contribute to bicycle dynamics, so that it is very important to measure it.

Contact patch areas were measured for different inflation pressure and vertical load on a reference road tyre, width 26 mm. Tests were

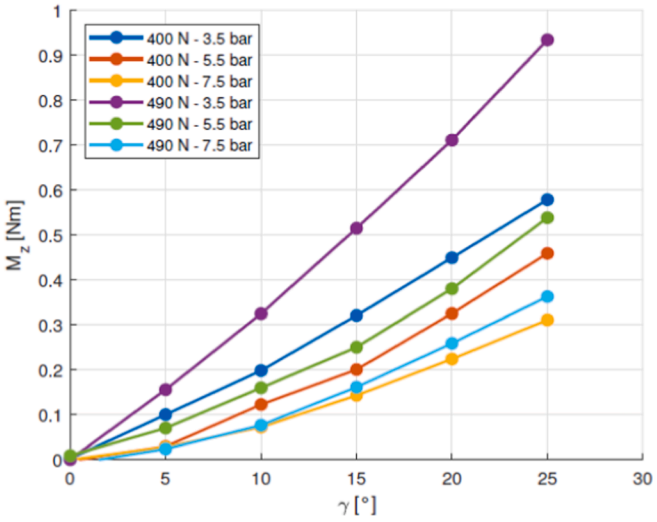

Fig. 4.1. . Experimental results of twisting torque obtained for a tyre of width 26 mm, inflated at 750 kPa. A vertical load of 490 N was applied. Values were recorded for camber angles in the range 0-25°.

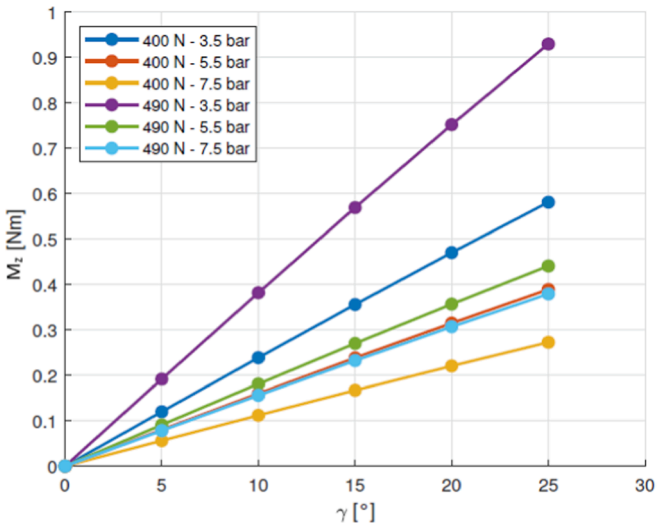

Fig. 4.2. . Twisting torque obtained from theoretical model. It was derived for different vertical loads (400 N and 490 N) and inflation pressures (range 3.5—7.5 bar).

carried out with *VeTyT* to measure the self-aligning torque by varying the camber angle and evaluate the twisting torque experimentally. The measured twisting torque was found to increase with increasing contact patch area, for the same value of camber angle.

A simplified model to predict the twisting torque was introduced. It was found to provide satisfying results in terms of accuracy. Nonetheless, it presents some limitations:

- It cannot be used for large camber angles. The elliptical approximation of the contact patch is not valid anymore.
- The model requires to know the dimensions of contact patch that have to be measured.
- A model able to predict the dimensions of contact patch specific for bicycle tyres has not been implemented yet. A study on the correlation between the contact patch area and the influence of parameters such as inflation pressure and vertical load has been carried out, and it could be a first step through the definition of a larger database.
- The longitudinal stiffness was assumed to be equal to the cornering stiffness, since we worked with limited slip angles. In addition, the longitudinal slips were assumed to be equal along the entire contact patch wide (i.e. constant in $\times$ direction, as defined in Fig. 3.2).
- The proportionality coefficient K_ε was assumed to be constant despite it may vary with inflation pressure and vertical load. Nonetheless, this approximation may provide a ready-to-use value for future analysis on road racing bicycle tyre. In this way, we are contributing to develop a database to enable parametric analysis of different bicycle tyres, complementing the work of Moore et al. [42,43].

The model presented in this paper was found to predict the trend and magnitude of the twisting torque for the most exploited range of camber angles (0-10°). Self-aligning torque and twisting torque for bicycle tyres are among the toughest characteristics to measure, since they are commonly featured by high uncertainty and poor signal-to-noise ratio. This simplified model tries to provide a rather simple way to predict twisting torque starting from the knowledge of cornering stiffness and contact patch area, usually easier to measure. It requires additional efforts to be refined, and in the future we may try to introduce smarter synthetic indexes.

CRediT authorship contribution statement

G. Dell'Orto: Conceptualization, Investigation, Data curation, Writing – original draft. **F.M. Ballo:** Conceptualization, Data curation, Software. **M. Gobbi:** Supervision. **G. Mastinu:** Supervision.

Declaration of Competing Interest

The authors declare that they have no known competing financial interests or personal relationships that could have appeared to influence the work reported in this paper.

Data availability

Data will be made available on request.

Acknowledgements

The authors thank Lorenzo Uslenghi, Lorenzo Vaccari, Prof. Gianantonio Magnani and Dr. Mario Pennati for their support during the months of hard work and test.

References

[1] European Environment Agency, "Annual Report 2019, EU policies - Energy," pp. 1–5, 2019.
[2] E. Union and C. I. Europe, "The state of national cycling strategies in Europe (2021)," 2021.
[3] EU Ministers for Transport, "Declaration on Cycling as a Climate Friendly Transport Mode," p. 5, 2015.
[4] A. Ari, et al., "Surging Energy Prices in Europe in the Aftermath of the War. How to Support the Vulnerable and Speed up the Transition Away From Fossil Fuels", 2022.
[5] S. Corwin, R. Zarif, A. Berdichevskiy, and D. Pankratz, "The futures of mobility after COVID-19. Scenarios for transportation in a postcoronavirus world," Deloitte Development LLC, pp. 1–21, 2020.
[6] Deloitte's TMT, "Technology, Media, and Telecommunications Predictions 2020." 2020. [Online]. Available: https://www2.deloitte.com/content/dam/insights/us/articles/722835_tmt-predictions-2020/DI_TMT-Prediction-2020.pdf.
[7] World Health Organization 2020, *Cyclist Safety: An Information Resource for Decision-Makers and Practitioners*, no. October. 2017.
[8] L.E.V.M. de Guerre, S. Sadiqi, L.P.H. Leenen, C.F. Oner, S.M. van Gaalen, Injuries related to bicycle accidents: an epidemiological study in The Netherlands, Eur. J. Trauma Emerg. Surg. 46 (2) (2020) 413–418, https://doi.org/10.1007/s00068-018-1033-5.
[9] O.V. Casas, R. Dalazen, A. Balbinot, 3D load cell for measure force in a bicycle crank, Measurement (Lond) 93 (Nov. 2016) 189–201, https://doi.org/10.1016/j.measurement.2016.07.031.
[10] M. Ambrož, Raspberry Pi as a low-cost data acquisition system for human powered vehicles, Measurement (Lond) 100 (Mar. 2017) 7–18, https://doi.org/10.1016/j.measurement.2016.12.037.
[11] J. Gao, A. Sha, Y. Huang, L. Hu, Z. Tong, W. Jiang, Evaluating the cycling comfort on urban roads based on cyclists' perception of vibration, J. Clean. Prod. 192 (Aug. 2018) 531–541, https://doi.org/10.1016/j.jclepro.2018.04.275.
[12] G. Dell'Orto, F.M. Ballo, G. Mastinu, Experimental methods to measure the lateral characteristics of bicycle tyres – a review, Veh. Syst. Dynam., pp. 1–23, Nov. 2022, http://doi.org/10.1080/00423114.2022.2144388.
[13] C.A. Manrique-Escobar, C.M. Pappalardo, D. Guida, On the Analytical and Computational Methodologies for Modelling Two-wheeled Vehicles within the Multibody Dynamics Framework: A Systematic Literature Review, J. Appl. Comput. Mech. 8 (1) (Jan. 2022) 153–181, https://doi.org/10.22055/jacm.2021.37935.3118.
[14] D. Gordon Wilson, T. Schmidt, J.M. Papadopoulos, Bicycle Science, 4th ed., MIT Press, 2020.
[15] A. Dressel and J. Sadauckas, Characterization and modelling of various sized mountain bike tires and the effects of tire tread knobs and inflation pressure, Appl. Sci. (Switzerland), vol. 10, no. 9, May 2020, http://doi.org/10.3390/app10093156.
[16] V.E. Bulsink, A. Doria, D. Van De Belt, B. Koopman, The effect of tyre and rider properties on the stability of a bicycle, Adv. Mech. Eng. 7 (12) (2015) Dec, https://doi.org/10.1177/1687814015622596.
[17] N. Baltus, About the mechanical properties of bicycle tyres, Thesis, Delft University of Technology, MSc, 2019.
[18] A. Doria, M. Tognazzo, G. Cusimano, V. Bulsink, A. Cooke, B. Koopman, Identification of the mechanical properties of bicycle tyres for modelling of bicycle dynamics, Veh. Syst. Dyn. 51 (3) (Mar. 2013) 405–420, https://doi.org/10.1080/00423114.2012.754048.

[19] A. E. Dressel, "Measuring and Modeling the Mechanical Properties of Bicycle Tires," PhD Thesis, University of Wisconsin-Milwaukee, 2013. [Online]. Available: https://dc.uwm.edu/etd/386.
[20] M. Gobbi, G. Mastinu, F. Comolli, F. Ballo, G. Previati, Motorcycle smart wheels for monitoring purposes, Bycicle Motorcycle Dynam. no. September (2019) 9–11.
[21] M. Bartolozzi, G. Savino, M. Pierini, Novel high-fidelity tyre model for motorcycles to be characterised by quasi-static manoeuvres–rationale and numerical validation, Veh. Syst. Dyn. 60 (12) (2022) 4290–4316, https://doi.org/10.1080/00423114.2021.2013506.
[22] V. Cossalter, A. Doria, R. Lot, N. Ruffo, M. Salvador, Dynamic properties of motorcycle and scooter tires: Measurement and comparison, Veh. Syst. Dyn. 39 (5) (May 2003) 329–352, https://doi.org/10.1076/vesd.39.5.329.14145.
[23] V. Cossalter, A. Doria, M. Formentini, M. Peretto, Experimental and numerical analysis of the influence of tyres properties on the straight running stability of a sport-touring motorcycle, Veh. Syst. Dyn. 50 (3) (2012) 357–375, https://doi.org/10.1080/00423114.2011.587520.
[24] H.B. Pacejka, Tire and Vehicle, Dynamics (2006), https://doi.org/10.1016/B978-0-7506-6918-4.X5000-X.
[25] V. Cossalter, A. Doria, The relation between contact patch geometry and the mechanical properties of motorcycle tyres, Veh. Syst. Dyn. 43 (SUPPL) (2005) 156–164, https://doi.org/10.1080/00423110500141045.
[26] V. Cossalter, A. Doria, E. Giolo, L. Taraborrelli, M. Massaro, Identification of the characteristics of motorcycle and scooter tyres in the presence of large variations in inflation pressure, Veh. Syst. Dyn. 52 (10) (2014) 1333–1354, https://doi.org/10.1080/00423114.2014.940981.
[27] M. Massaro, V. Cossalter, G. Cusimano, The effect of the inflation pressure on the tyre properties and the motorcycle stability, Proc. Inst. Mech. Eng., Part D: J. Autom. Eng. 227 (10) (2013) 1480–1488, https://doi.org/10.1177/0954407013496231.
[28] R. Lot, A Motorcycle Tire Model for Dynamic Simulations: Theoretical and Experimental Aspects, Meccanica 39 (3) (Jun. 2004) 207–220, https://doi.org/10.1023/B:MECC.0000022842.12077.5c.
[29] V. Cossalter, A. Doria, R. Lot, Steady Turning of Two-Wheeled Vehicles, Veh. Syst. Dyn. 31 (3) (1999) 157–181, https://doi.org/10.1076/vesd.31.3.157.2013.
[30] V. Cossalter, Motorcycle Dynamics. 2006.
[31] G. Dell'Orto, F.M. Ballo, G. Mastinu, M. Gobbi, Bicycle tyres – Development of a new test-rig to measure mechanical characteristics, Measurement (Lond) 202 (Oct. 2022), https://doi.org/10.1016/j.measurement.2022.111813.
[32] L. Uslenghi, L. Vaccari, Indoor testing of cycling tyres and quality assurance of 'Vetyt' test rig, MSc, Thesis, Politecnico di Milano, 2021.
[33] S. Derafshpour, M. Valizadeh, A. Mardani, and M. Tamaddoni Saray, A novel system developed based on image processing techniques for dynamical measurement of tire-surface contact area, Measurement (Lond), vol. 139, pp. 270–276, Jun. 2019, http://doi.org/10.1016/j.measurement.2019.02.074.
[34] C. Zhang, W. Zhao, W. Wang, J. Zhang, Vision-based tire deformation and vehicle-bridge contact force measurement, Measurement (Lond) 183 (Oct. 2021), https://doi.org/10.1016/j.measurement.2021.109792.
[35] A. Swami, C. Liu, J. Kubenz, G. Prokop, and A. K. Pandey, Experimental Study on Tire Contact Patch Characteristics for Vehicle Handling with Enhanced Optical Measuring System, SAE Int. J. Veh. Dyn. Stab. NVH, vol. 5, no. 3, Apr. 2021, http://doi.org/10.4271/10-05-03-0023.
[36] C.A. Schneider, W.S. Rasband, K.W. Eliceiri, NIH Image to ImageJ: 25 years of image analysis, Nat. Methods 9 (7) (2012) 671–675, https://doi.org/10.1038/nmeth.2089.
[37] M.D. Abràmoff, P.J. Magalhães, S.J. Ram, Image processing with imageJ, Biophotonics Int. 11 (7) (2004) 36–41, https://doi.org/10.1201/9781420005615.ax4.
[38] I.J.M. Besselink, A.J.C. Schmeitz, H.B. Pacejka, An improved Magic Formula/Swift tyre model that can handle inflation pressure changes, Veh. Syst. Dyn. 48 (SUPPL. 1) (2010) 337–352, https://doi.org/10.1080/00423111003748088.
[39] G. Mastinu, M. Fainello, Study of the Pneumatic Tyre Behaviour on Dry and Rigid Road by Finite Element Method, Veh. Syst. Dyn. 21 (3) (1992) 143–165.
[40] J.P. Pauwelussen, in: J.P. Pauwelussen (Ed.), Essentials of Vehicle Dynamics, Butterworth-Heinemann, Oxford, 2015, pp. 7–74, https://doi.org/10.1016/B978-0-08-100036-6.00002-9.
[41] G. Mastinu, M. Ploechl, Road and off-Road Vehicle System dynamics Handbook, Taylor & Francis Group, LLC, 2014.
[42] J.K. Moore, M. Hubbard, A.L. Schwab, and J.D.G. Kooijman, Accurate Measurement of Bicycle Parameters, Bicycle and Motorcycle Dynamics: Symposium on the Dynamics and Control of Single Track Vehicles, no. October, pp. 20–22, 2010.
[43] M. Hubbard, J.K. Moore, R. Gilboa, A. Kubicki, A. Toribio, and J.K. Moore, Practical Realization of a Theoretical Optimal-Handling Bicycle, 2019, http://doi.org/10.6084/m9.figshare.9883328.v1.